Skeletal Radiology (2019) 48:1765–1773
https://doi.org/10.1007/s00256-019-03219-8

SCIENTIFIC ARTICLE

Evaluation of giant cell tumors by diffusion weighted imaging–fractional ADC analysis

Oganes Ashikyan[1] · M. Chalian[1] · D. Moore[1] · Y. Xi[1] · P. Pezeshk[1] · A. Chhabra[1,2]

Received: 6 February 2019 / Revised: 13 March 2019 / Accepted: 8 April 2019 / Published online: 19 April 2019

Abstract

Background A single ADC value is used in clinical practice on multi b-value acquisitions. Low b-value acquisitions are affected by intravoxel incoherent motion, which is dependent on perfusion. Giant cell tumors (GCTs) are known to exhibit early arterial enhancement and low ADC values. Mean, minimum and fractional ADC characteristics of osseous and tenosynovial GCTs are systematically evaluated.

Methods Tenosynovial and osseous GCTs were included. Each lesion was evaluated on conventional MRI and DWI by two musculoskeletal radiologists. ADC was measured by placing an ROI on the most confluent enhancing portion of the lesion. Fractional and best fit ADC calculations were performed using MATLAB software.

Results No statistically significant difference was found between tenosynovial and osseous lesions' ADC values. Mean ADC for all lesions was 1.0×10^{-3} mm^2/s (SD = 0.2×10^{-3} mm^2/s) and minimum ADC was 0.5×10^{-3} mm^2/s (SD = 0.3×10^{-3} mm^2/s). Average mean ADC value obtained from B50–B400 slope was 1.1×10^{-3} mm^2/s (SD = 0.2×10^{-3} mm^2/s), and the average mean ADC value obtained from B400–B800 slope was 0.8×10^{-3} mm^2/s (SD = 0.1×10^{-3} mm^2/s) [p-value <0.01].

Conclusion Tenosynovial and osseous GCTs demonstrate similar and low ADC values, which become even lower when using high b-value pairs. Our study also supports the theory of intravoxel incoherent motion that becomes apparent at low b values as related to giant cell tumors, which are known to be hyperperfused.

Keywords Giant cell tumor · Tenosynovial · Osseous · DWI · MRI

Introduction

Giant cell tumors (GCTs) of bone and tenosynovial GCTs are two histologically different neoplasms with some overlapping characteristics. One of these is hyper perfusion [1]. In this study, we use the term "osseous GCT" to describe intraosseous GCTs and their rare soft tissue counterpart. The term "tenosynovial GCT" is used to describe GCTs in tendon sheath, bursa, and intra-articular locations. Pigmented villonodular synovitis (PVNS) is another term used to describe intra-articular tenosynovial GCTs.

The GCTs are non-invasively evaluated using radiographs and conventional MRI, and in cases of soft tissue lesions, ultrasound [2]. Osseous and tenosynovial GCTs demonstrate mixed MRI signal characteristics. The lesions may show homogeneous or heterogenous enhancement on delayed post-gadolinium imaging [3] and can mimic bone and soft tissue sarcomas.

Dynamic MRI and diffusion weighted imaging (DWI) were studied by various groups to better non-invasively evaluate musculoskeletal neoplasms [1, 4–6]. Rapid arterial enhancement and washout of osseous GCTs on dynamic MRIs has been described in an English language report [7] as part of a large study of 100 musculoskeletal neoplasms, and in a German study [8] of nine patients with GCTs. PVNS and GCTs of tendon sheaths are also known to be hypervascular [2, 9].

Diffusion weighted imaging (DWI) is another tool for the evaluation of bone and soft tissue lesions [10, 11]. Previous

✉ Oganes Ashikyan
Oganes.Ashikyan@UTSouthwestern.edu

[1] Department of Radiology, Musculoskeletal Imaging, UT Southwestern Medical Center, 5323 Harry Hines Blvd, E230-C, Dallas, TX 75390-9316, USA

[2] Department of Orthopedic Surgery, UT Southwestern Medical Center, Dallas, TX, USA

case reports and studies that included GCT among other neoplasms showed low apparent diffusion coefficient (ADC) values in osseous GCT and their soft tissue counterpart [12, 13]. To our knowledge, diffusion characteristics of tenosynovial GCTs have not been systematically reported in English language literature. Low ADC values in a Chinese study of PVNS [14] have been reported after analysis of 7 cases.

The diffusion characteristics can be complicated by perfusion effects in the vascularized tumor. Effects of perfusion on MR diffusion measurements have been described in detail by Iima and Le Bihan [15]. The most widely accepted hypothesis postulates that DWI obtained with b-values below 200–400 s/mm^2 is affected by tissue microcapillary perfusion [15]. In the domain of musculoskeletal tumors, the effect of using different pairs of b-values and different calculation methods to derive ADC has not been systematically evaluated.

The purpose of this study was to derive ADC values of osseous and tenosynovial GCTs using different calculation methods and different b-values. We hypothesized:

1. ADC values are different when calculations are derived from different b-value pairs.
2. ADC values obtained from B50 and B800 slope are equivalent to ADC value obtained using least squares calculation.
3. There is no difference in ADC values between intraosseous and tenosynovial GCTs.

Methods

This study was a cross-sectional, retrospective, HIPAA-compliant evaluation that was performed after the institutional review board approval. The informed consent requirement was waived.

Subjects

The electronic medical records were searched from January 2015 to October of 2018 (Fig. 1). Initial report search included terms "giant cell" and was limited to extremity MRIs. This was followed by search of pathology reports for final diagnosis of "giant cell tumor." Patients between the ages of 18 and 89 as per HIPAA "Safe Harbor" guideline for de-identifying health information and with no history of prior surgery in the area of neoplasm were included in this study. To be included, the MRI studies had to contain B = 50, B = 400 and B = 800 DWI acquisitions in addition to routine T1W, T2W images, and pre-contrast and post-contrast fat saturated T1W images.

Image acquisition

The images were acquired on 1.5 and 3 T Siemens and Phillips scanners using extremity coils and following our institutional musculoskeletal tumor evaluation protocol. Our routine musculoskeletal oncology protocol includes at least one plane of T1W and at least two planes of fat-saturated T2W sequences, DWI, and pre-contrast and post-contrast fat suppressed T1W imaging. Post-contrast subtracted images were obtained by subtracting pre-contrast images from post-contrast images. DWI images were uniformly acquired using B = 50, B = 400, and B = 800 values in all cases. The following parameters were used for DWI acquisition: TR = 8,900 ms, TE = 75 ms; slice thickness = 4 mm, FOV = 180–280 mm, receiver bandwidth = 1698 Hz/pixel, imaging time = 4 min. The individual b-values and machine calculated ADC maps were routinely available in PACS (picture archiving and communications system.)

Two scans of tenosynovial GTCs were obtained on 1.5-T magnets, while the remaining lesions were imaged on 3 T magnets. Four of the soft tissue lesions were imaged on Phillips Achieva 3 T scanner (Best, Netherlands) and two tenosynovial GCTs were imaged on 1.5-T Siemens Avanto scanner, remaining four tenosynovial GCTs and all bone lesions were imaged on Siemens 3 T Skyra scanner (Erlangen, Germany).

Image analysis and ADC calculations

Two readers—musculoskeletal radiologists with 10 and 2 years of post-fellowship experience—reviewed T1W, fat suppressed T2W, and pre-contrast and post-contrast images including post-contrast subtraction images to determine part of the lesion that demonstrated nodular or mass-like post contrast enhancement, and to avoid sampling clearly fluid filled areas such as loculations with fluid-fluid levels. We also avoided sampling septations and lesional areas that were clearly hypointense on both DWI and ADC. All b-value images were also reviewed to determine the portion of the neoplasm that demonstrated clearly high signal on DWI. DICOM tags 0019,100C (Siemens) and 0018,0098 (Phillips) on each DWI image were manually examined to confirm the correct labeling of different b images.

The b-value images from the same axial slice location were saved in the DICOM format and imported into MATLAB 2018a software. An in-house workflow algorithm was created for image analysis using MATLAB image processing toolbox. The regions of interest (ROI) were drawn on the ADC image calculated from B50–B800 acquisitions independently by the two radiologists. Mean and minimum ADC values were calculated using the two b-value pairs: B50–B400 and B400–B800. ADC values were also calculated from B50–B800 using simple slope between the two points approach and the

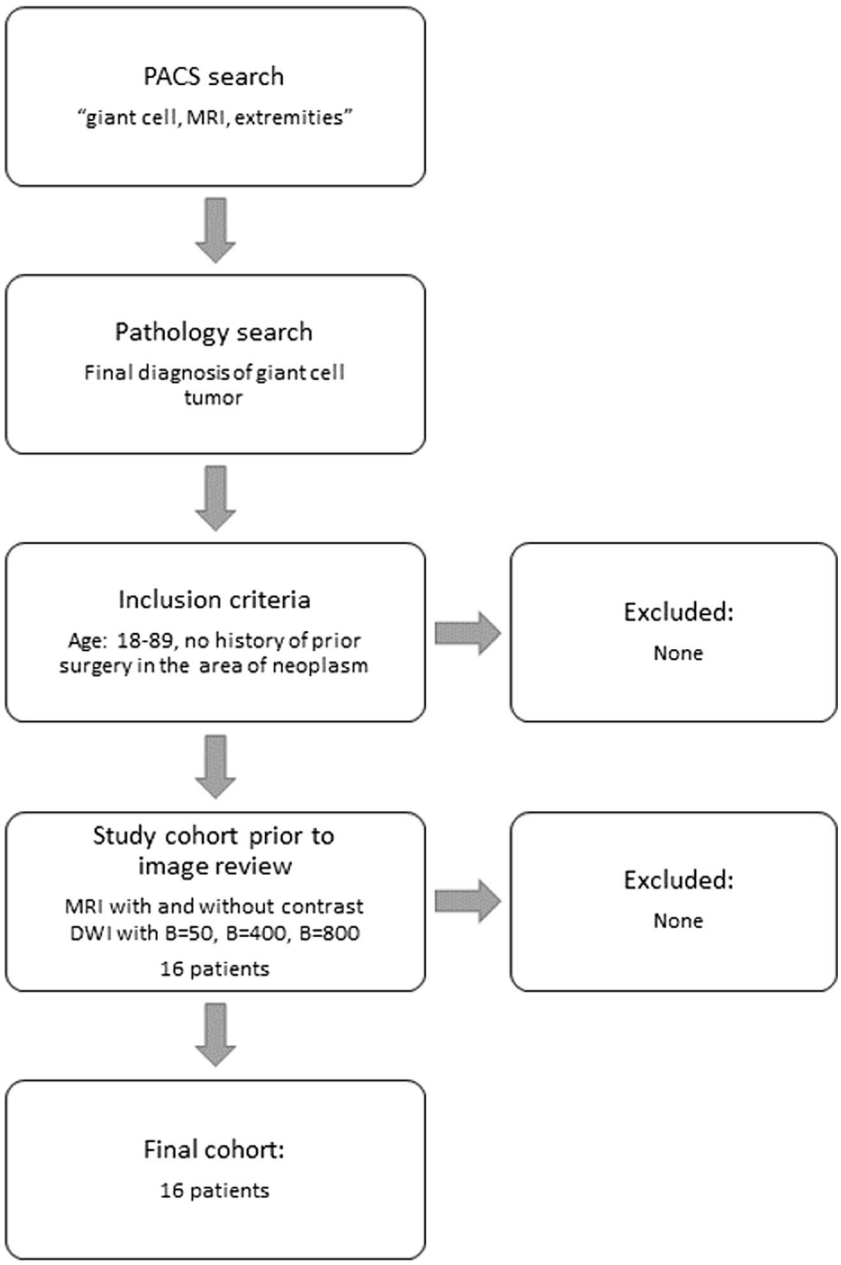

Fig. 1 Subjects selection flowchart

best fit least squares approximation approach using all three b values. The original ROI mask was used for all calculations, which corresponded to exactly the same pixels on each b-value acquisition, as similar protocols with all three b values were applied during a single sequence on all scanners.

The musculoskeletal reader with 10 years of post-graduate experience systematically recorded conventional MRI signal characteristics of the lesions including appearance on T1W, fat saturated T2W images, presence or absence of hypointense rim around the lesion, presence or absence of fluid-fluid levels, and pattern of post-contrast enhancement.

Statistical analysis

The de-identified data was stored on a Microsoft Excel 2010 spreadsheet. The measurements obtained by the two readers were averaged prior to the statistical analysis. Descriptive and analytical statistics were obtained including mean, median and standard deviations (SD) for ADC obtained at various b-values pairs. Paired student t-test for population with unequal variance was used to determine the statistically significant difference between ADC values obtained at low and high b-value pairs. This was calculated for both minimum ADC and for mean ADC values. Box plots were generated using R

studio. Intraclass correlation coefficients (ICC) were calculated using the irr package in R [16, 17].

Bland Altman plot was generated for comparison of B50-B800 slope calculation to the best fit line using the least squares method. Welch two sample TOST method was used to evaluate equivalence of ADC calculations between the tenosynovial and osseous neoplasms. A *P*-value of <0.05 was considered statistically significant.

Results

Subjects and tumors

There were seven female and nine male patients with an average age of 38.8 years (median = 34 years, SD = 16.4 years). Ten patients presented with tenosynovial GCTs and 6 patients presented with intraosseous GCTs. The average size of the tenosynovial GCTs was 1.9 cm (median = 1.7 cm, SD = 0.8 cm), and intraosseous neoplasms was 8.4 cm (median = 8.6 cm, SD = 2.3 cm). The average number of days from MRI to tissue diagnosis was 42 days (median = 27 days, SD = 40 days).

Conventional MRI

On conventional MRI, most of the tenosynovial GCTs demonstrated heterogeneous, slightly hyperintense appearance on fat saturated T2W images with a thin dark rim outlining the margins in 90% of the tenosynovial GCTs (9/10 lesions) and 83% of osseous neoplasms (5/6 lesions). Both tenosynovial GCTs and osseous GCTs demonstrated heterogenous, mixed appearance on T1W images. Eighty-three percent of osseous neoplasms (5/6 lesions) demonstrated the presence of loculations with fluid-fluid levels (ABC components). There were three patterns of late post contrast enhancement, which are described in Table 1.

ADC values

ADC values obtained from least squares approximation of slope between the three b-value acquisitions based on the average signal intensity of the ROI were very similar to the simple slope calculation between the B50 and B800 acquisitions (Fig. 2). There were three tenosynovial lesions and three osseous neoplasms that demonstrated 0.1×10^{-3} mm^2/s difference between these two approaches. Overall, the mean ADC for all lesions was 1.0×10^{-3} mm^2/s (SD = 0.2×10^{-3} mm^2/s) for both calculations. Average minimum ADC was 0.5×10^{-3} mm^2/s (SD = 0.3×10^{-3} mm^2/s) based on B50–B800 calculation. The minimum ADC values for least squares best fit line approach were not obtained, as our algorithm first averaged the signal intensities in each ROI prior to line fitting portion of the algorithm.

Table 1 Contrast enhancement characteristics of GCTs

	No enhancement	Solid	Heterogenous
Tenosynovial GCTs	2/10 (20%)	1/10 (10%)	7/10 (70%)
Osseous GCTs	0/6 (0%)	1/6 (17%)	5/6 (83%)

Tenosynovial GCTs vs osseous GCTs

The mean ADC and standard deviation of tenosynovial neoplasms using the least squares calculation were 0.9×10^{-3} mm^2/s (SD = 0.1×10^{-3} mm^2/s). The mean ADC and standard deviation of tenosynovial neoplasms using the simple B50–B800 slope calculation were 0.9×10^{-3} mm^2/s (SD = 0.2×10^{-3} mm^2/s).

The mean ADC and standard deviation for osseous neoplasms using simple B50–B800 slope and using least squares calculation were 1.1×10^{-3} mm^2/s (SD = 0.3×10^{-3} mm^2/s).

P-values were 0.1 for three b-value least-squares approach, and 0.3 for simple slope two-b-value approach comparing mean ADC of tenosynovial and osseous neoplasms.

Minimum ADC for tenosynovial neoplasms was 0.5×10^{-3} mm^2/s (SD = 0.2×10^{-3} mm^2/s) using simple B50–B800 slope approach. Minimum ADC for osseous neoplasms was 0.2×10^{-3} mm^2/s (SD = 0.7×10^{-3} mm^2/s) using the same calculation. *P*-value was 0.6 comparing minimum ADC of tenosynovial and bone GCTs. Equivalence Welch TOST test comparing tenosynovial and osseous neoplasms for various b-value calculations demonstrated equivalent mean ADC values for both groups (Table 2).

Fractional ADC analysis

Average mean ADC value obtained from B50–B400 slope was 1.1×10^{-3} mm^2/s (SD = 0.2×10^{-3} mm^2/s) and the average mean ADC value obtained from B400–B800 slope was 0.8×10^{-3} mm^2/s (SD = 0.1×10^{-3} mm^2/s; Fig. 3). The *p*-value was <0.01.

Average minimum ADC value obtained from B50–B400 slope was 0.4×10^{-3} mm^2/s (SD = 0.5×10^{-3} mm^2/s) and the average minimum ADC value obtained from B400–B800 slope was 0.3×10^{-3} mm^2/s (SD = 0.4×10^{-3} mm^2/s). The *p*-value was 0.10.

Inter-reader agreement

The agreements between the two readers for mean and minimum ADC values were moderate to good for most of different calculations of ADC (Table 3).

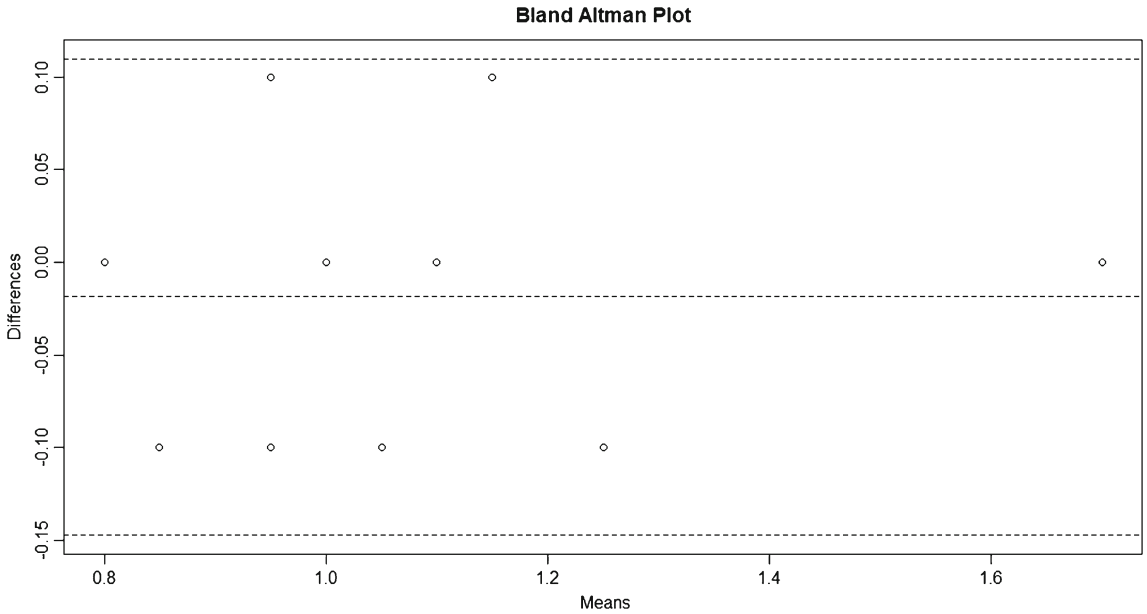

Fig. 2 Bland Altman Plot. Mean ADC calculations based on B50–B800 slope and ADC calculation based on the best fit least squares approach is within 0.1×10^{-3} mm^2/s for each pair of measurements. Identical mean ADC measurements for different subjects with no difference are shown as a single open dot

Discussion

In this largest series focused on GCTs of bones and tendon sheaths, we confirm the findings of previous case reports that overall ADC values of GCTs are quite low. In general, it is believed that malignant hypercellular neoplasms such as sarcomas and lymphomas demonstrate low ADC values, while benign neoplasms present with higher ADC values [10, 11]. This study confirms that an overlap between the malignant and benign conditions exists and GCT is such an example with low ADC values. It is difficult to pinpoint the exact reason for low ADC values in GCTs, but several theories are plausible. First, the presence of hemosiderin and other blood products in these neoplasms likely affects the ADC measurements. While we took great care to avoid sampling clearly hemorrhagic components, it is possible that microscopic areas of hemorrhagic products were present in the sampled pixels. Other potential reasons for low ADC measurements in GCTs include the nature of intra-lesional matrix or presence of hypercellular components.

Our fractional ADC analysis revealed several interesting findings. First, ADC calculations from low b-value pairs were higher than the ADC calculations from high b-value pairs. Lee et al. [13] also found similar results in their case report of GCT, where ADC values were thought to be related to hyper-perfusion in these neoplasms. These results also correspond well to LeBihan's theory of intravoxel incoherent motion (IVIM) expected at low b values, thought to be related to perfusion effects [15]. GCTs are known to present with hyper-perfusion characteristics on previous dynamic studies

Table 2 Comparison of ADC value calculations between soft tissue and osseous neoplasms. Unpaired Welch Two Sample TOST test with confidence level of 95%

	Tenosynovial vs bone Welch two-sample TOST test								
	Slope	DF	P-value	Null hypothesis	CIL	CIH	Mean soft	Mean bone	SE Diff
Mean	B50–B800	6.4	0.00	Rejected	−0.5	0.1	0.9	1.1	0.1
	B50–B400	7.3	0.00	Rejected	−0.5	0.1	1.0	1.2	0.1
	B400–B800	10.3	0.00	Rejected	−0.2	0.0	0.8	0.9	0.1
Min.	B50–B800	6.2	0.00	Rejected	−0.2	0.4	0.6	0.5	0.2
	B50–B400	6.0	0.03	Rejected	−0.3	0.9	0.5	0.2	0.3
	B400–B800	7.9	0.01	Rejected	−0.3	0.6	0.4	0.2	0.3
Least squares		6.3	0.00	Rejected	−0.5	0.0	0.9	1.2	0.1

Legend: *DF* degrees of freedom, *CIL* low bound of confidence interval, *CIH* high bound of confidence interval, *SE Diff* standard error of the difference

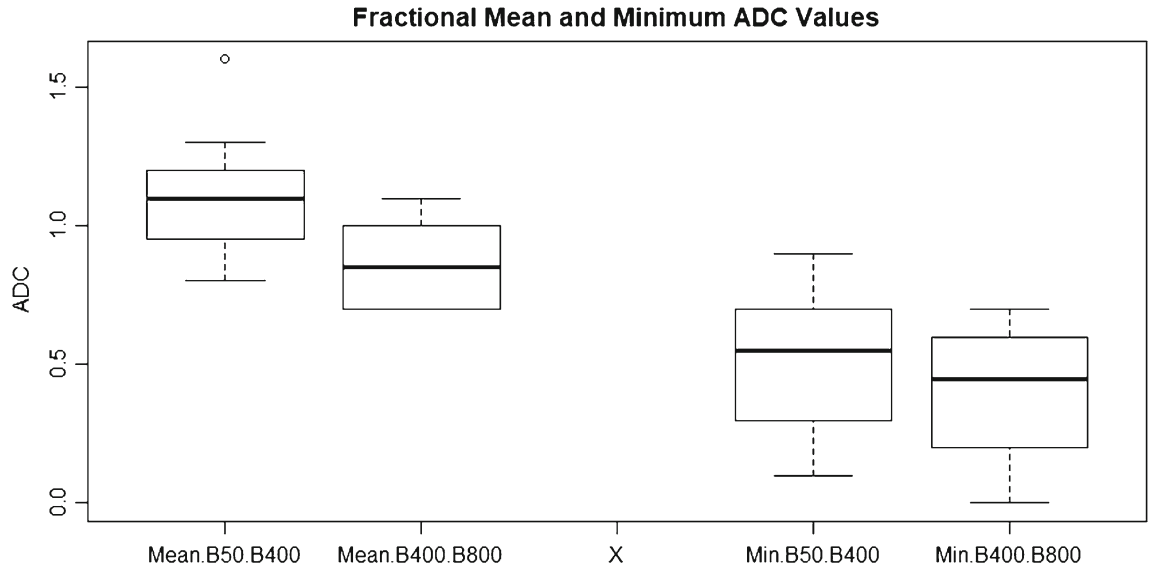

Fig. 3 Fractional mean and minimum ADC values. Mean.B50.B400 = mean ADC calculated for B50–B400 pair; Mean.B400.B800 = mean ADC calculated for B400–B800 pair; Min.B50.B400 = minimum ADC calculated for B50–B400 pair; Min.B400.B800 = minimum ADC calculated for B400–B800 pair

[7, 8]. Future systematic studies will be needed to confirm these hyperperfusion effects in other musculoskeletal tumors apart from GCTs using dedicated IVIM techniques. Furthermore, we demonstrate that high b-value pairs generate overall low ADC values. This suggests that for protocols where dynamic post contrast sequence is obtained, it may be reasonable to eliminate low b values from acquisition to minimize overall study time. Optimal b-value selection would be, however, a subject of future research in different neoplasms.

It is important to consider whether mean or minimum ADC should be used for characterization of musculoskeletal neoplasms. In this study, we were able to show statistically significant difference for the mean ADC values from low and high b-value pair calculations, but not for the minimum ADC value calculations. Our results also show relatively wider range of standard deviation for minimum ADC calculations. Both phenomena are likely explained by simple noise that becomes important for pixels with very low ADC values. In theory, it should be impossible for any regions in a tumor to exhibit ADC values below zero. However, based on the nature of ADC equation that simply reflects a slope of signal intensity drop, nothing stops an ADC calculation algorithm from calculating a negative ADC if a given pixel is contaminated by random noise. It is unknown how each vendor of clinical analysis software deals with this problem as information about specifics of code and algorithm is usually proprietary. Until such calculations are standardized across all vendors, radiologists should consider both mean and minimum ADC values, realizing that at the lower end of spectrum, ADC calculations may be contaminated by random noise.

Table 3 Two Reader Intraclass Correlational Coefficient (ICC)

	ICC	95% confidence interval	
Mean ADC B50–B800	0.70	0.35	0.88
Mean ADC B50–B400	0.67	0.29	0.87
Mean ADC B400–B800	0.27	−0.23	0.66
Minimum ADC B50–B800	0.63	0.23	0.85
Minimum ADC B50–B400	0.81	0.54	0.93
Minimum ADC B400–B800	0.78	0.48	0.91
Least squares ADC	0.61	0.19	0.84

Careful attention to placement of ROI for ADC measurement is very important in clinical practice and in research. ROI should be placed over parts of neoplasms that are least contaminated by septations, hemorrhage, and cystic components. The sampled regions should demonstrate high signal on corresponding DWI (Fig. 4) to avoid artificially lowering ADC value of a region.

What is the clinical utility of our findings? First, it is important for a radiologist to understand that various methods can be used to calculate ADC values and careful attention needs to be paid to what exact b values are used by local software. It is important to understand that a potential for discrepancies may exist among various vendor's implementations. To our knowledge, there is no single standard method that has been agreed to. Second, if the theory of IVIM is confirmed by other larger studies that include a variety of lesions, dynamic contrast enhanced sequences can potentially be replaced by fractional ADC analysis. Conversely, low b-value acquisition can be eliminated in cases where dynamic contrast enhanced sequences are obtained.

We were not able to document difference in ADC values between the tenosynovial and osseous neoplasms. While we

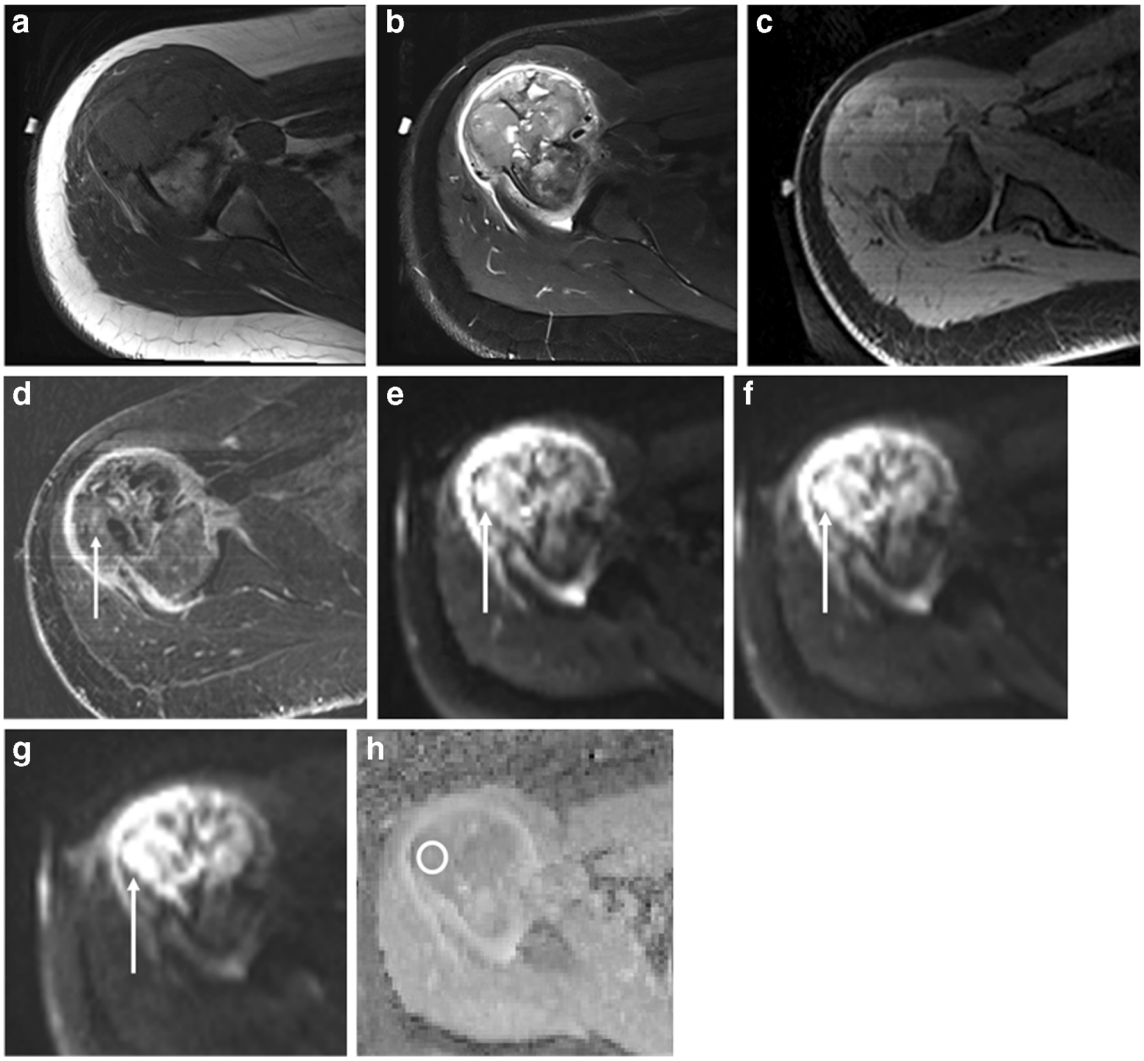

Fig. 4 Example of ROI selection for ADC analysis. T1W (A) and T2W (B) images demonstrate a heterogenous exophytic mass in the right humerus. Pre-contrast (C) and subtracted post-contrast (D) fat-saturated T1W images demonstrate enhancing (arrow in D) and non-enhancing components of the lesion. B50, B400 and B800 images (E, F, G) show hyperintense components (arrows) corresponding to areas of restricted diffusion. ROI is placed on ADC image (circle in H) over solid appearing enhancing component carefully avoiding fluid filled and septated areas. Notice the pixelated appearance of the ADC image. In this study, we used original DWI DICOM data for ADC image calculation and did not use any filters for smoothing or other post-processing of ADC image

realize that the small number of subjects in this study may affect the power of statistical analysis, we would like to discuss differences and similarities between osseous and tenosynovial GCTs. Definitions and nomenclature related to giant cells tumors (GCTs) can be confusing. Based on the histological appearance and the site of origin, these are broadly grouped into osseous GCTs and tenosynovial (or synovial) GCTs. Tenosynovial-type GCTs are further subdivided into tendon sheath GCTs, intra-articular GCTs (PVNS) and intra-bursal GCTs.

Osseous-type GCTs can be further subdivided into truly intra-osseous GCTs and their soft tissue counter-part, so-called "soft tissue GCT." While many soft tissue GCTs of osseous type represent recurrence of primary intra-osseous GCTs, some authors reported rare isolated soft tissue GCTs [18]. Recent genomics analysis suggested that soft tissue GCTs may represent yet additional subtype of GCT different from their osseous counterpart [19].

It is generally known that osseous and tenosynovial GCTs demonstrate different histopathological characteristics. However, one study that investigated ultrastructural cytochemical features of cells in bone, tendon sheath, and intra-articular GCTs found similarities of tartrate-resistant acid phosphatase (TRAP)-positive cells in all three tumor types. As such, common cell lineage was proposed despite different histopathological appearance for all three of the studied types of GCTs [20].

Interestingly, intra-osseous GCTs and tenosynovial GCTs have other overlapping imaging and pathological characteristics. Similar to intra-osseous GCT, tendon-sheath associated

GCTs demonstrate the presence of osteoclast-like giant cells [21–25], and similar to GCTs of tendon sheaths [26], GCTs of bones contain large amounts of hemosiderin [27].

We acknowledge the following limitations of our study. The sample size was moderate in this project and the power of statistical analysis can be affected by the sample size. However, this is the largest sample in the currently available literature that describes diffusion characteristics of GCTs. We used DWI images from various scanners and it is possible that ADC calculations can be affected by the way data is acquired, transmitted, processed and stored by various vendors. From another perspective, all the images used in this study were obtained on Phillips and Siemens scanners only. Whether our results can be easily translated to data acquired on other scanners is unclear at this time.

Conclusion

Osseous and tenosynovial GCTs demonstrate similar and low ADC values, which even become lower when using high b-value pairs. This supports the theory of intravoxel incoherent motion that becomes apparent at low b values as related to GCTs, which are known to be hyperperfused.

Compliance with ethical standards

Disclosures O. Ashikyan, MD contributes content to, and his family member owns a business that manages the following websites: www.mridoc.com; www.newagepub.com; www.solrevs.com.

A. Chhabra, MD serves as a consultant with ICON Medical and Treace Medical Inc. A. Chhabra, MD also receives book royalties from Jaypee and Wolters.

Conflict of interest None.

IRB approval This study was a cross-sectional, retrospective, HIPAA-compliant evaluation that was performed after the institutional review board approval.

References

1. Verstraete KL, Lang P. Bone and soft tissue tumors: the role of contrast agents for MR imaging. Eur J Radiol. 2000;34:229–46.
2. Middleton WD, Patel V, Teefey SA, Boyer MI. Giant cell tumors of the tendon sheath: analysis of sonographic findings. AJR. 2004;183:337–9.
3. Thammaroj P, Chowchuen P, Sumananont C, Nasang T. MRI findings of giant cell tumor of tendon sheath and other benign soft tissue tumors in hand. J Med Assoc Thail. 2016;99:816–22.
4. Sujlana P, Skrok J, Fayad LM. Review of dynamic contrast-enhanced MRI: technical aspects and applications in the musculoskeletal system. J Magn Reson Imaging. 2018;47:875–90.
5. Choi YJ, Lee IS, Song YS, Kim JI, Choi KU, Song JW. Diagnostic performance of diffusion-weighted (DWI) and dynamic contrast-enhanced (DCE) MRI for the differentiation of benign from malignant soft-tissue tumors. J Magn Reson Imaging. 2019. https://doi.org/10.1002/jmri.26607.
6. Nagata S, Nishimura H, Uchida M, et al. Diffusion-weighted imaging of soft tissue tumors: usefulness of the apparent diffusion coefficient for differential diagnosis. Radiat Med. 2008;26:287–95.
7. Verstraete KL, De Deene Y, Roels H, Dierick A, Uyttendaele D, Kunnen M. Benign and malignant musculoskeletal lesions: dynamic contrast-enhanced MR imaging—parametric "first-pass" images depict tissue vascularization and perfusion. Radiology. 1994;192:835–43.
8. Libicher M, Bernd L, Schenk JP, Mädler U, Grenacher L, Kauffmann GW. Characteristic perfusion pattern of osseous giant cell tumor in dynamic contrast-enhanced MRI (in German). Radiologe. 2001;41:577–82
9. Barile A, Sabatini M, Iannessi F, Di Cesare E, Splendiani A, Calvisi V, et al. Pigmented villonodular synovitis (PVNS) of the knee joint: magnetic resonance imaging (MRI) using standard and dynamic paramagnetic contrast media. Report of 52 cases surgically and histologically controlled. Radiol Med. 2004;107:356–66.
10. Chhabra A, Ashikyan O, Slepicka C, Dettori N, Hwang H, Callan A, et al. Conventional MR and diffusion-weighted imaging of musculoskeletal soft tissue malignancy: correlation with histologic grading. Eur Radiol. 2018. https://doi.org/10.1007/s00330-018-5845-9.
11. Ahlawat S, Fayad LM. Diffusion weighted imaging demystified: the technique and potential clinical applications for soft tissue imaging. Skelet Radiol. 2018;47:313–28.
12. Pekcevik Y, Kahya MO, Kaya A. Diffusion-weighted magnetic resonance imaging in the diagnosis of bone tumors: preliminary results. J Clin Imaging Sci. 2013;3:63.
13. Lee MY, Jee WH, Jung CK, Yoo IR, Chung YG. Giant cell tumor of soft tissue: a case report with emphasis on MR imaging. Skelet Radiol. 2015;44:1039–43.
14. Li Y, Lou H, Wang R, et al. MRI-pathologic correlation of pigmented villonodular synovitis. Chin J Radiol. 2003;37:493–8.
15. Iima M, Le Bihan D. Clinical intravoxel incoherent motion and diffusion MR imaging: past, present, and future. Radiology. 2016;278:13–32.
16. Gamer M, Lemon J, Fellows I, Singh P. (2012). irr: Various coefficients of interrater reliability and agreement. R package version 0.84. https://CRAN.R-project.org/package=irr
17. R Core Team (2017). R: A language and environment for statistical computing. R Foundation for Statistical Computing, Vienna, Austria. https://www.R-project.org/.
18. Asotra S, Sharma S. Giant cell tumor of soft tissue: cytological diagnosis of a case. J Cytol. 2009;26:33–5.
19. Lee JC, Liang CW, Fletcher CD. Giant cell tumor of soft tissue is genetically distinct from its bone counterpart. Mod Pathol. 2017;30:728–33.
20. Anazawa U, Hanaoka H, Shiraishi T, Morioka H, Morii T, Toyama Y. Similarities between giant cell tumor of bone, giant cell tumor of tendon sheath, and pigmented villonodular synovitis concerning ultrastructural cytochemical features of multinucleated giant cells and mononuclear stromal cells. Ultrastruct Pathol. 2006;30(3):151–8.
21. Mahendra G, Kliskey K, Athanasou NA. Immunophenotypic distinction between pigmented villonodular synovitis and haemosiderotic synovitis. J Clin Pathol. 2010;63:75–8.
22. Neale SD, Kristelly R, Gundle R, Quinn JM, Athanasou NA. Giant cells in pigmented villo nodular synovitis express an osteoclast phenotype. J Clin Pathol. 1997;50:605–8.
23. Wood GS, Beckstead JH, Medeiros LJ, Kempson RL, Warnke RA. The cells of giant cell tumor of tendon sheath resemble osteoclasts. Am J Surg Pathol. 1988;12:444–52.

24. Lau YS, Sabokbar A, Gibbons CL, Giele H, Athanasou N. Phenotypic and molecular studies of giant-cell tumors of bone and soft tissue. Hum Pathol. 2005;36:945–54.
25. Taylor R, Kashima TG, Knowles H, et al. Osteoclast formation and function in pigmented villonodular synovitis. J Pathol. 2011;225: 151–6.
26. Murphey MD, Rhee JH, Lewis RB, Fanburg-Smith JC, Flemming DJ, Walker EA. Pigmented villonodular synovitis: radiologic-pathologic correlation. Radiographics. 2008;28:1493–518.
27. Aoki J, Moriya K, Yamashita K, et al. Giant cell tumors of bone containing large amounts of hemosiderin: MR-pathologic correlation. J Comput Assist Tomogr. 1991;15:1024–7.